Available online at website: https://journal.bcrec.id/index.php/bcrec

Bulletin of Chemical Reaction Engineering & Catalysis, 21 (3) 2026, 604-616

Original Research Article

Influence of Ni/CeO_2 on Pyrolytic Conversion of FOBS to Hydrogen Formation

Wan Nur Anis Amira Wan Ranizang[1], Mazura Jusoh[1], Mohd Asmadi[1], Zaki Yamani Zakaria[1,2,*]

[1]Department of Chemical Engineering, Faculty of Chemical and Energy Engineering, Universiti Teknologi Malaysia, 81310 Johor Bahru, Johor, Malaysia.
[2]Centre of Education Engineering (CEE), Universiti Teknologi Malaysia, 81310 Johor Bahru, Johor, Malaysia.

Received: 2nd March 2026; Revised: 10th April 2026; Accepted: 10th April 2026
Available online: 24th April 2026; Published regularly: October 2026

Abstract

Fuel Oil Blended Stock (FOBS) is a residual byproduct from petroleum refineries that is often underutilized and may cause storage and environmental issues. Converting FOBS into hydrogen through catalytic pyrolysis offers a sustainable waste valorisation pathway; however, no studies have focused on Ni/CeO_2 catalysts for hydrogen production from FOBS, which establishes the novelty of this work. This study aims to evaluate the performance of a Ni/CeO_2 catalyst for hydrogen production from FOBS via catalytic pyrolysis. A 3% Ni/CeO_2 catalyst was synthesized using the wet impregnation method and characterized using XRD, FESEM, BET, and FTIR. Catalytic pyrolysis experiments were conducted in a tubular furnace reactor at temperatures between 400-600 °C, nitrogen flow rates of 40-140 mL/min, and catalyst-to-feedstock ratios of 1:5, 1:10, and 1:15. The gaseous products were analyzed using GC-TCD/FID. The results showed that higher temperatures and catalyst-to-feedstock ratios improved FOBS conversion and hydrogen selectivity, with optimal performance achieved at 600 °C, 90 mL/min, and a catalyst-to-feedstock ratio of 1:15, yielding high conversion, gas yield, and hydrogen selectivity. In conclusion, the Ni/CeO_2 catalyst shows strong potential for converting FOBS into hydrogen-rich gas, supporting waste valorisation and sustainable hydrogen production.

Keywords: fuel oil blended stock ; hydrogen ; pyrolysis ; catalyst ; valorisation; Ni/CeO_2

How to Cite: Wan Ranizang, W. N. A. A., Jusoh, M., Asmadi, M., Zakaria, Z. Y. (2026). Influence of Ni/CeO_2 on Pyrolytic Conversion of FOBS to Hydrogen Formation. *Bulletin of Chemical Reaction Engineering & Catalysis*, 21 (3), 604-616. (DOI: 10.9767/bcrec.20677)

Permalink/DOI: https://doi.org/10.9767/bcrec.20677

1. Introduction

Hydrogen (H_2) is widely regarded as a clean and sustainable energy carrier that can support the transition toward low-carbon energy systems. Traditionally, hydrogen is primarily produced from fossil fuels via conventional processes such as steam reforming, which raises concerns regarding environmental impact and long-term resource sustainability [1]. Therefore, alternative hydrogen production methods were searched and it was discovered that using waste-derived feedstocks have gained increasing attention due to their potential to address energy demand and waste management issues simultaneously. One potential waste feedstock is fuel oil blended stock (FOBS), a refinery-derived residue that contains a high concentration of hydrocarbons and recoverable energy [2,3]. FOBS is commonly treated as waste and disposed of through incineration, which leads to environmental pollution and the loss of valuable resources [4]. Converting FOBS into hydrogen could provide a sustainable solution for the valorization of refinery waste and the production of clean energy.

Several hydrogen production technologies have been developed, including electrochemical, biological, and thermochemical methods [1]. Among these methods, thermochemical

* Corresponding Authors.
Email: zakiyamani@utm.my (Z.Y. Zakaria)

conversion is considered more suitable for hydrocarbon-rich wastes due to its ability to process complex and heterogeneous feedstocks [5]. Pyrolysis is widely used because it operates in an oxygen-free environment and allows better control of product distribution. Previous studies have shown that pyrolysis of petroleum-based wastes, such as heavy oil, refinery sludge, waste lubricants, and plastic residues, can produce hydrogen-rich gas [6,7,8]. These findings indicate that refinery residues are suitable feedstocks for thermochemical hydrogen production.

The efficiency of pyrolysis for hydrogen production is highly dependent on the catalyst used. Previous studies have reported that zeolite catalysts and metal-based catalysts can significantly influence product distribution and hydrogen yield by promoting cracking, reforming, and dehydrogenation reactions [9,10]. Nickel (Ni)-based catalysts are widely known for their strong dehydrogenation activity and ability to enhance hydrogen formation. Meanwhile, cerium oxide (CeO_2) has attracted attention as a catalyst support due to its oxygen storage capacity, redox properties, and ability to reduce coke formation [11,12]. The combination of Ni and CeO_2 has demonstrated promising performance in hydrogen production processes such as steam reforming and pyrolysis-gasification, suggesting that this catalyst system has strong potential for hydrogen production from hydrocarbon-based waste [13].

Despite these promising developments, most previous studies have focused on biomass, plastics, and general petroleum residues, while only limited studies have investigated hydrogen production specifically from FOBS. Furthermore, the application of Ni/CeO_2 catalysts in the catalytic pyrolysis of FOBS for hydrogen production has not been widely reported, and the influence of catalyst loading and operating parameters on hydrogen yield from FOBS is still not well understood. Therefore, this research focuses on hydrogen production from FOBS via catalytic pyrolysis using Ni/CeO_2 catalysts. The novelty of this research lies in the application of Ni/CeO_2 catalysts specifically for FOBS feedstock and the evaluation of the effects of catalyst loading and operating parameters on hydrogen production. This study is important for providing new knowledge on refinery waste valorization and catalytic hydrogen production from complex hydrocarbon waste.

Hence, the objectives of this research are to synthesize and characterize Ni/CeO_2 catalysts and to evaluate their performance for hydrogen production from FOBS via catalytic pyrolysis by investigating the effect of operating parameters on hydrogen yield.

2. Materials and Methods

2.1. Materials

This study employed FOBS as the primary feedstock, which was collected from refinery waste generated by a multinational petrochemical refinery based in Johor, Malaysia. The catalyst precursors, nickel(II) nitrate hexahydrate (99.9%) and cerium(IV) oxide (<5 µm, 99.9% trace metals basis), were purchased from Sigma-Aldrich.

2.2. Synthesis of catalyst

The 3 wt.% Ni/CeO_2 catalyst was prepared using the impregnation technique with nickel(II) nitrate hexahydrate ($Ni.(NO_3)_2.6H_2O$) and cerium(IV) oxide (CeO_2) as starting materials. No further purification of the reagents was performed. The preparation began by dispersing CeO_2 in deionized water under continuous stirring to form a uniform suspension. $Ni.(NO_3)_2.6H_2O$ was then added to the suspension, and the mixture was stirred for 2 hours at 80 °C to promote uniform distribution of nickel ions over the support material. The resulting mixture was subsequently dried to remove excess water and then ground into fine particles. Finally, the calcination step was conducted at 550 °C for 6 hours to obtain a stable crystalline structure, which is essential for enhancing the catalyst's performance.

2.3 Characterization of Catalyst

The synthesized catalysts (CeO_2 and 3wt.% Ni/CeO_2) were characterized to determine their structural, morphological, textural, and functional properties. Crystalline structure analysis was carried out using X-ray diffraction (XRD) on a Rigaku SmartLab diffractometer, with patterns recorded over a 2θ range of 10° to 80° at a scanning rate of 0.02 °.min^{-1}. Before XRD analysis, samples were thermally treated and evenly placed on a glass slide to ensure accurate diffraction data. The surface morphology of the catalysts was examined using a Hitachi SU8020 Field Emission Scanning Electron Microscope (FESEM), operated at an accelerating voltage range of 2-10 kV. The CeO_2 and 3%Ni/CeO_2 samples were analyzed directly, whereas the Ni sample was first calcined for 3 hours to remove moisture and stored in a desiccator before imaging. For imaging, the samples were evenly spread on carbon tape mounted on a specimen stub and coated with a thin layer of conductive material, such as gold, to enhance image clarity, reduce charging effects, and prevent thermal damage. Textural analysis, including BET surface area, pore volume, average pore diameter, and pore size distribution, was performed using a Micromeritics Tristar II BET analyzer. Prior to

measurement, the samples were degassed under vacuum at 300 °C for 1 hour to remove moisture and surface contaminants. Functional groups present in the catalyst were identified using Fourier Transform Infrared (FTIR) spectroscopy with a Perkin-Elmer Spectrum GX instrument, covering the range of 4,000 to 650 cm^{-1}. For FTIR sample preparation, a small amount of catalyst powder was mixed with potassium bromide (KBr), then compressed into a transparent pellet using a hydraulic press. The pellet was subsequently analyzed to detect specific IR absorption bands corresponding to the functional groups present in the catalyst.

2.4. Pyrolysis Setup and Experimental Conditions

The experimental procedure began by weighing 10 grams of FOBS and adding an appropriate amount of catalyst according to the desired C/F ratio, followed by mixing in a ceramic crucible. FOBS and catalyst were layered and thoroughly blended to ensure uniform contact. The crucible was then placed at the center of a quartz tube within a tubular reactor, which was housed in a stainless-steel chamber insulated with glass wool. To maintain an inert atmosphere, nitrogen gas was continuously supplied through the system. Pyrolysis was conducted at controlled heating rates of 10-30 °C/min across a temperature range of 400-600 °C. Reaction times at 60 minutes, with nitrogen flow rates set between 40-140 mL/min, and catalyst-to-feedstock ratios of 1:5, 1:10, and 1:15. During pyrolysis, volatile compounds were released and directed through a condensation unit, where the end-products were separated into liquid and gas fractions. Figure 1 illustrates the schematic diagram for the pyrolysis system in this study [14].

The gas products were collected in sampling bags and analyzed using gas chromatography (GC-TCD/FID), enabling precise quantification of H_2 and other light gases. This data served as a critical metric for evaluating the catalytic performance and optimizing conditions for H_2-rich

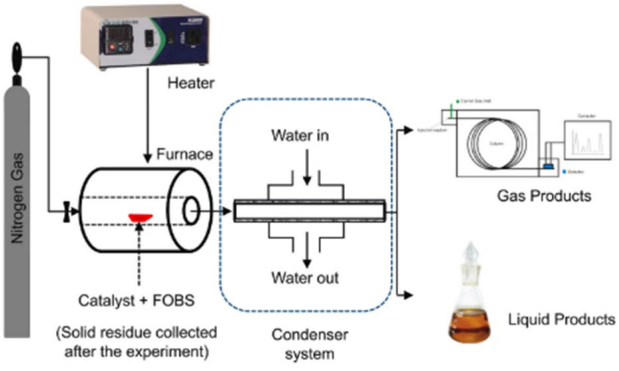

Figure 1. Pyrolysis system [14].

gas formation. Liquid products were collected primarily for overall yield assessment. Solid residues, comprising unconverted feedstock and spent catalysts, were collected to support the overall mass balance. Product yields were determined gravimetrically. FOBS conversion, along with the yields of liquid (Y_l), solid (Y_s), gas (Y_g), and selectivity of hydrogen (S_{H2}), were calculated using Equations (1)-(5).

$$Conversion\ of\ FOBS\ (\%) = \frac{(m_{feedstock})-(m_s)_{final}-mass\ of\ catalyst}{m_{feedstock}} \times 100\% \quad (1)$$

$$Liquid\ yield\ (\%): Y_l = \frac{\sum \text{mliq (products)}}{\text{mliq (in)}} \times 100\% \quad (2)$$

$$Solid\ yield\ (\%): Y_s = \frac{m_s - \text{mass of catalyst}}{\text{mliq (in)}} \times 100\% \quad (3)$$

$$Gas\ yield\ (\%): Y_G = 100\% - Y_l - Y_s \quad (4)$$

$$H_2\ Selectivity\ (\%): S_{H_2} = \frac{w_{H_2}}{\sum w_{total\ hydrocarbon\ gas}} \times 100\% \quad (5)$$

3. Results and Discussion

3.1. Characterizations of Catalyst

Catalyst characterization for CeO_2 and 3%Ni/CeO_2 was carried out using XRD, FESEM, BET, and FTIR analysis. This analysis aimed to examine the structural catalyst and obtain essential information for interpreting their performance in catalytic pyrolysis experiments.

3.1.1. Phase structure and crystallinity analysis

XRD analysis was conducted to investigate the crystal structures and phases of Ni, CeO_2, and 3%Ni/CeO_2. The corresponding XRD patterns are shown in Figure 2. Figure 2 presented the X-ray diffraction (XRD) patterns of raw nickel (Ni), raw ceria (CeO_2), and the modified catalyst containing 3wt.% Ni supported on CeO_2 (3%Ni/ CeO_2). The XRD pattern of raw Ni exhibits sharp and intense diffraction peaks, indicating a high degree of crystallinity. According to the JCPDS database, the diffraction peaks observed at 2θ values of approximately 37.2°, 43.3°, and 62.9° can be attributed to the characteristic reflections of NiO, confirming the crystalline nature of the nickel oxide phase.

For raw CeO_2, the diffraction peaks located at 2θ values of 28.6° (111), 33.1° (200), 47.5° (220), 56.3° (311), 59.1° (222), and 69.4° (400) correspond well to the cubic fluorite structure of ceria. The absence of additional diffraction peaks indicates that the CeO_2 support is phase-pure and highly crystalline. For the 3%Ni/ CeO_2 catalyst, the characteristic fluorite structure of CeO_2 is well preserved after Ni incorporation, indicating that the support framework remains intact during

catalyst synthesis. No distinct diffraction peaks corresponding to NiO are detected in the modified catalyst, although a noticeable reduction in peak intensity is observed compared to raw CeO_2. This observation may be attributed to the low Ni loading and the high dispersion of Ni species on the CeO_2 surface, which renders the NiO crystallites either too small or too highly dispersed to be detected by XRD. In addition, the results suggest that Ni species are predominantly located on the surface of CeO_2 rather than forming a Ni-Ce solid solution, supported by the fact that the fluorite lattice of ceria remains structurally stable.

CeO_2 was selected as a catalyst support is due to its structural stability and its ability to promote the formation of oxygen vacancies through the reversible Ce^{4+}/Ce^{3+} redox cycle [15]. Smaller CeO_2 crystallites tend to enhance the generation of surface oxygen vacancies because of lattice distortion and the reduced coordination of surface oxygen atoms. These characteristics improve oxygen mobility and facilitate reactant activation through synergistic metal – support interaction [16]. Therefore, the combination of nanocrystalline CeO_2, abundant oxygen vacancies, and well-dispersed Ni species is expected to increase the density of catalytically active sites, thereby significantly enhancing catalytic performance.

To further support these findings, the crystallite sizes of raw Ni, raw CeO_2, and the 3%Ni/CeO_2 catalyst were estimated using the Scherrer equation, $D = \frac{K\lambda}{\beta cos\theta}$ [17]. The calculated average crystallite sizes were 72.37 nm for raw Ni, 49.17 nm for raw CeO_2, and 70.19 nm for the 3%Ni/CeO_2 catalyst. The increase in crystallite size observed for the modified catalyst after Ni loading suggests the successful incorporation of Ni onto the CeO_2 support, which may be associated with particle growth or aggregation during catalyst synthesis. Overall, the XRD results confirm the successful preparation of the 3%Ni/CeO_2 catalyst with a preserved CeO_2 crystal structure and well-dispersed Ni species.

3.1.2. Surface morphology analysis

FESEM was used to observe the surface structure of the Ni, CeO_2, and 3% Ni/CeO_2 catalysts, and the image displayed in Figure 3. FESEM images taken at a scale of 1 µm revealed

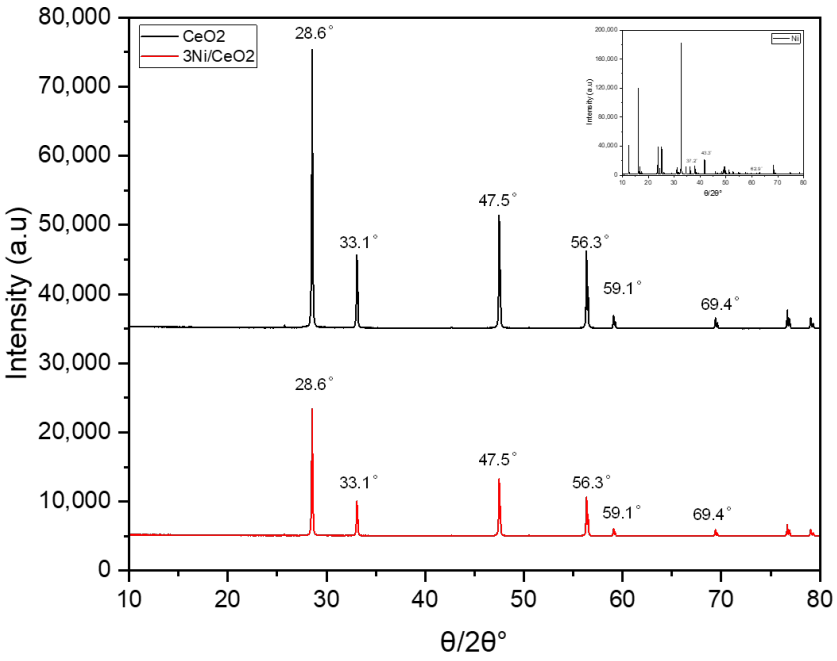

Figure 2. XRD patterns for raw Ni, raw CeO_2, and modified catalyst, 3%Ni/CeO_2.

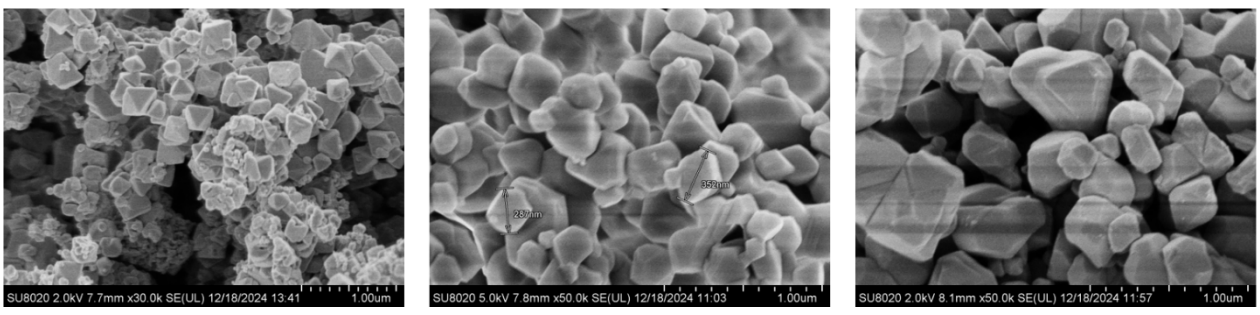

Figure 3. FESEM images for (a) Ni, (b) CeO_2, and (c) 3wt% Ni/CeO_2.

distinct morphological characteristics for each sample. The Ni sample consisted of relatively uniform particles with sharp edges. The well-defined shapes and uniformity suggest good crystallinity and indicate that the synthesis process was well-controlled. In contrast, the CeO_2 sample exhibited a more irregular and heterogeneous surface morphology. The particles were less distinctly shaped and tended to form agglomerates. This tendency toward agglomeration is typical for cerium oxide and is attributed to its high surface energy and reactive surface sites [18].

For the modified catalyst, the 3%Ni/CeO_2 sample exhibited a noticeable shift in morphology. The particles became more uniformly shaped, and the surface was smoother and more structured compared to pure CeO_2. The morphology closely resembled that of the Ni sample, suggesting successful dispersion of nickel throughout the ceria matrix. No isolated Ni particles were observed, indicating that the metal was either highly dispersed or incorporated at a scale below the detection limit of the FESEM at this magnification. These structural modifications may enhance catalytic properties by increasing surface accessibility and strengthening metal-support interactions.

3.1.3. Textural properties analysis

BET analysis was performed to complement the XRD and FESEM results by evaluating the surface characteristics of the catalysts, including surface area (SA), total pore volume (TPV), micropore volume (MicroV), and mesopore volume (MesoV). As reported previous study, a higher surface area typically provides more active sites, which can improve the overall catalytic performance [19]. The BET results for raw Ni, raw CeO_2, and the modified 3%Ni/CeO_2 catalysts are summarized in Table 1. As shown in Table 1, the BET analysis revealed that the raw Ni catalyst exhibited the highest surface area (12.6650 m^2/g) and total pore volume (0.034208 cm^3/g), indicating a highly porous structure that is favourable for catalytic activity. In contrast, CeO_2 showed the lowest surface area (2.2547 m^2/g) and pore volume (0.00124 cm^3/g), reflecting its naturally compact structure. For the modified catalyst, the incorporation of 3 wt.% Ni onto the CeO_2 support led to a slight increase in surface area (2.6654 m^2/g) and total pore volume (0.00189 cm^3/g) compared to pure CeO_2, suggesting that the addition of Ni contributed to a mild enhancement of the textural properties.

Table 1. BET porosity data.

Catalyst	Surface area (m^2/g)	TPV (cm^3/g)	MicroV (cm^3/g)	MesoV (cm^3/g)
Ni	12.6650	0.034208	0.002777	0.031431
CeO_2	2.2547	0.001240	0.000369	0.000871
3%Ni/CeO_2	2.6654	0.001890	0.000315	0.001575

Analysis of the pore structure further revealed that Ni incorporation increased the mesopore volume from 0.000871 cm^3/g for CeO_2 to 0.001575 cm^3/g for 3%Ni/CeO_2, indicating improved mesoporosity. This enhancement is expected to facilitate reactant diffusion and improve catalytic efficiency. A previous study reported that the stronger metal-support interactions may influence the catalyst's redox behaviour and stability [20].

Based on the N_2 adsorption-desorption isotherms in Figure 4, raw Ni exhibited a Type III isotherm, while raw CeO_2 and the modified 3%Ni/CeO_2 catalyst displayed Type II isotherms. The Type II isotherm indicates that the 3%Ni/CeO_2 catalyst possesses a nonporous or macroporous structure, with pore sizes typically larger than 50 nm [21]. Such large pores facilitate the diffusion of reactants and products, making the catalyst particularly suitable for the decomposition of bulky molecules such as FOBS. In addition, this structural characteristic is capable of reducing mass transfer limitations and minimizing pore blockage and coke formation during the catalytic process.

3.1.4. Vibrational spectroscopy analysis

The FTIR spectra of Ni, CeO_2 and 3%Ni/CeO_2 catalysts exhibit several notable differences that

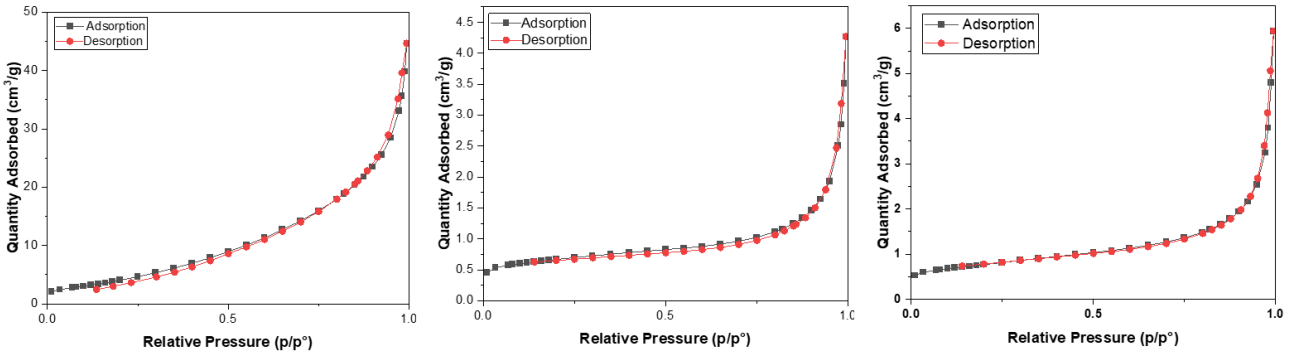

Figure 4. N_2 adsorption-desorption isotherms of catalysts.

reflect structural and surface modifications induced by nickel incorporation, as shown in Figure 5.

The FTIR spectrum of the raw Ni catalyst is characterized by high transmittance across the entire wavenumber range, with an absorption band observed in the hydroxyl stretching region at 3600-3200 cm^{-1} [22]. This band is attributed to the stretching vibrations of surface hydroxyl (-OH) groups, which are most likely associated with residual moisture or hydroxyl species remaining from the nickel precursor, $Ni(NO_3)_2.6H_2O$. In addition, absorption bands in the range of 1800-1650 cm^{-1} correspond to Ni-N-O vibrational modes, confirming the presence of nickel-containing species. These observations indicate that the raw Ni catalyst predominantly exists as a bulk oxide, as there is no other significant peak appeared across the wavenumber range.

For the raw CeO_2 catalyst, a broad absorption band observed between 3330-3270 cm^{-1} is attributed to the O-H stretching vibrations of surface hydroxyl groups and adsorbed water molecules, reflecting the oxygen-active nature of ceria. The broadness of this band suggests the presence of hydrogen-bonded hydroxyl groups on the surface, which are known to enhance catalytic redox activity by facilitating oxygen mobility. Furthermore, absorption bands in the range of 1760-1665 cm^{-1} can be assigned to Ce-O stretching vibrations, confirming the characteristic lattice vibrations of the ceria framework.

The FTIR spectrum of the 3%Ni/CeO_2 catalyst exhibits a broad absorption band between 3400 and 3200 cm^{-1}, corresponding to the O-H stretching vibrations of surface hydroxyl groups and adsorbed water molecules [23]. This band broadens compared to raw CeO_2, reflecting the influence of Ni incorporation on the surface hydroxyl environment. In the region of 1673-1629 cm^{-1}, the appearance of Ni-Ce-O vibrational bands indicates strong interaction between Ni species and the CeO_2 support, confirming the successful integration of Ni into the ceria lattice. Importantly, the absence of absorption bands associated with organic residues, such as C=O groups, confirms the effectiveness of the calcination step and the complete removal of precursor-related organics [24]. Overall, these spectral changes demonstrate that Ni was successfully incorporated onto the ceria surface, while preserving the oxygen-active nature of the support, which is essential for enhanced catalytic performance.

3.2. Catalytic Pyrolysis Hydrogen Production

In this study, the catalytic pyrolysis process for hydrogen production was investigated using 3%Ni/CeO_2. Blank experiment (no catalyst) and ceria were used as references to evaluate the performance of the modified catalyst. The catalytic performance of 3%Ni/CeO_2 in hydrogen production is closely related to the physicochemical properties of the catalyst, as determined by XRD, FESEM, BET and FTIR analyze. The XRD analysis confirmed the presence of NiO species well dispersed on the CeO_2 support, which indicated successful incorporation of active metal sites responsible for hydrocarbon cracking and reforming reactions during pyrolysis. The FESEM images showed that Ni particles were uniformly distributed on the ceria surface, providing more accessible active sites and enhancing catalyst and FOBS interaction, which contributes to higher hydrogen yield. BET surface area analysis demonstrated that the catalyst possessed sufficient surface area and pore structure, which are important for improving the catalyst diffusion and increasing the contact between FOBS vapors and active catalytic sites. In addition, FTIR analysis confirmed the presence of functional groups and

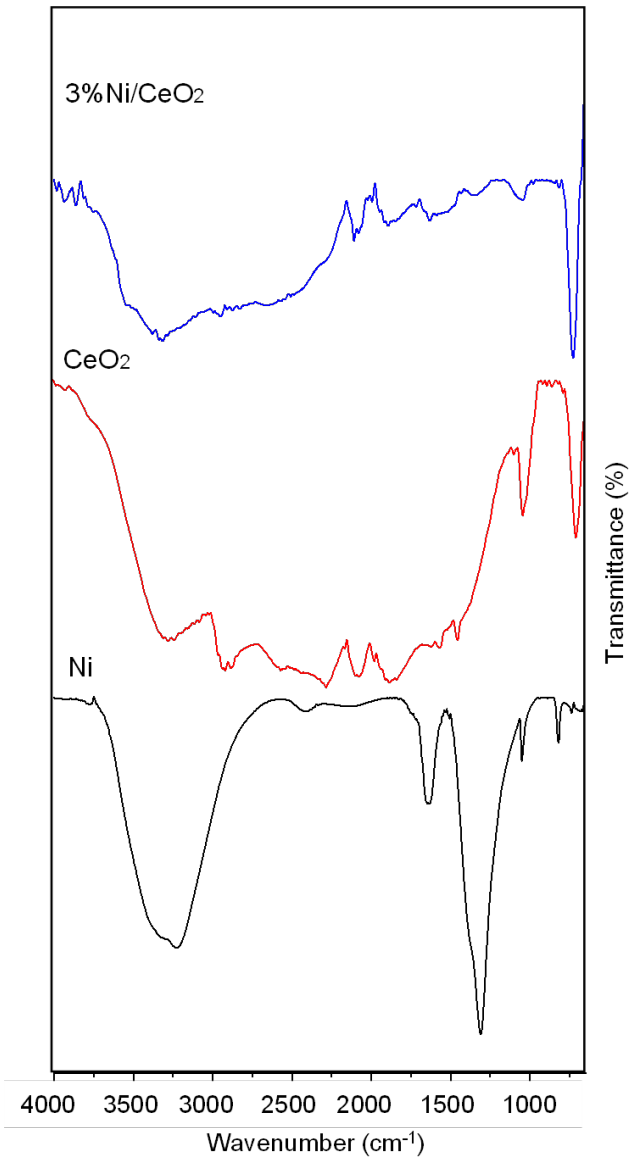

Figure 5. FTIR spectra for (a) Ni, (b) CeO_2 and (c) 3 wt.% Ni/ CeO_2.

metal-oxygen bonding (Ni-O-Ce), which suggests a strong metal-support interaction that improves catalyst stability and reduces metal sintering during high-temperature pyrolysis. Therefore, the combination of good metal dispersion, adequate surface area, and strong metal-support interaction explained the improved catalytic performance of 3%Ni/CeO_2 in enhancing hydrogen production.

The study focused on three main parameters: the C/F ratio, reaction temperature, and nitrogen flow rate. These factors play a crucial role in enhancing the breakdown of FOBS during pyrolysis and in producing valuable products, particularly hydrogen. The C/F ratio reflects how effectively the catalyst can decompose FOBS in the pyrolysis system. Temperature is also critical, as it provides the energy necessary to break down the complex structure of FOBS, with optimal temperatures required to achieve efficient decomposition. Although the nitrogen flow rate is less critical, it is still important for maintaining the smooth operation of the system. Previous studies have suggested a general range for nitrogen flow, but the exact value must be determined, as different tubular reactors may require different flow rates. In this study, the C/F ratios were set at 1:5, 1:10, and 1:15, the reaction temperature ranged from 400 °C to 600 °C, and the nitrogen flow rate was varied between 40 mL/min and 140 mL/min.

3.2.1. Influence of catalyst-to-feedstock (C/F) ratios (1:5, 1:10, 1:15)

The effect of the C/F ratio was investigated at ratios of 1:5, 1:10, and 1:15. During this study, the reaction temperature was fixed at 500 °C, and the nitrogen flow rate was maintained at 90 mL/min. The resulting conversion, yield, and selectivity data are presented in Table 2. Table 2 presents the conversion, product yields (solid, liquid, and gas), and hydrogen selectivity obtained at different C/F ratios using CeO_2 and 3%Ni/CeO_2 catalysts, with a blank (no catalyst) experiment included for comparison. In the absence of a catalyst, the conversion was limited to 64.8%, accompanied by a relatively high solid yield. This indicates incomplete cracking of FOBS during non-catalytic pyrolysis, where thermal decomposition alone was insufficient to effectively break down the complex feedstock structure.

At a C/F ratio of 1:5, the introduction of catalysts improved conversion compared to the blank run. CeO_2 achieved a conversion of 69.3%, while 3%Ni/CeO_2 showed a comparable conversion of 68.3%. Despite similar conversion levels, the product distributions differed notably between the two catalysts. CeO_2 favored gas formation, resulting in a higher gas yield of 37.3% and a hydrogen selectivity of 53.3%. In contrast, 3%Ni/CeO_2 produced higher solid and liquid yields, suggesting that the catalytic activity of nickel was not fully utilized at a 1:5 ratio. This behavior may be attributed to the relatively high catalyst loading relative to the feedstock, as 2 g of catalyst was introduced for only 10g of FOBS, potentially leading to poor catalyst-feedstock contact or mass transfer limitations.

At a C/F ratio of 1:10, a good improvement in conversion was observed for both catalysts. In the presence of CeO_2, the conversion increased to 78.8%, while the 3%Ni/CeO_2 catalyst exhibited a higher conversion of 81.8%. This increasing trend in conversion was parallel by a corresponding increase in gas yield and hydrogen selectivity. For CeO_2, the gas yield reached 37.3% with a hydrogen selectivity of 50.7%, whereas 3%Ni/CeO_2 produced a significantly higher gas yield of 53.8% along with an enhanced hydrogen selectivity of 64.0%. Simultaneously, a noticeable reduction in solid and liquid yields was observed for both catalysts, indicating more effective cracking of heavy FOBS components into lighter gaseous products. Increasing the C/F ratio to 1:10 improved catalytic performance, particularly for the modified catalyst, 3%Ni/CeO_2, thereby promoting deeper cracking reactions and enhancing hydrogen-rich gas production.

Lastly, at a C/F ratio of 1:15, both catalysts achieved high conversion levels, exceeding 80%. CeO_2 alone resulted in a conversion of 81.1%,

Table 2. Conversion, yield, and selectivity at C/F ratios of 1:5, 1:10, and 1:15.

C/F Ratio	Catalyst	Conv. (%)	Y_s (%)	Y_l (%)	Y_g (%)	S_{H2}(%)
-	Blank (no catalyst)	64.8	48.0	23.0	29.0	29.3
1:5	CeO_2	69.3	30.7	32.0	37.3	53.3
	3%Ni/CeO_2	68.3	40.2	39.0	20.8	40.9
1:10	CeO_2	78.7	21.3	30.0	37.3	50.7
	3%Ni/CeO_2	81.8	18.2	28.0	53.8	64.0
1:15	CeO_2	81.1	18.9	34.0	47.1	49.2
	3%Ni/CeO_2	89.8	10.2	20.1	69.6	76.3

**Conv.: Conversion; Y_s: Yield solid; Y_l: Yield liquid; Y_g: Yield gas; S_{H2}: Selectivity of Hydrogen

whereas 3%Ni/ CeO_2 reached a higher conversion of 89.8%. At this ratio, gas yield and hydrogen selectivity also increased significantly, reaching 47.1% and 69.6%, respectively, while solid and liquid yields decreased. This trend indicates that increasing the C/F ratio provides more active sites, promoting deeper cracking reactions and favoring the formation of hydrogen-rich gases. In addition, only 0.67 g of Ni was loaded onto 10 g of FOBS at this ratio, which is relatively low compared to other conditions, yet it was sufficient to achieve the highest conversion, gas yield, and hydrogen selectivity. The superior performance of 3%Ni/CeO_2 can likely be attributed to an increase in surface area upon Ni loading, as supported by BET data. The higher surface area provides more accessible active sites, enhancing the catalytic efficiency and significantly promoting hydrogen formation during pyrolysis. Previous studies have reported that the presence of an appropriate amount of catalyst can help overcome kinetic limitations and promote reforming reactions, thereby enhancing hydrogen yield [25].

Overall, the catalytic pyrolysis of FOBS demonstrated that both CeO_2 and 3%Ni/CeO_2 significantly enhance conversion and hydrogen production compared to non-catalytic pyrolysis. Increasing the C/F ratio from 1:5 to 1:15 led to higher conversion, greater gas yield, and improved hydrogen selectivity, while solid and liquid yields decreased, indicating more effective cracking of the feedstock. Among the catalysts tested, 3%Ni/CeO_2 consistently outperformed CeO_2 alone, achieving the highest conversion (89.8%), gas yield (47.1%), and hydrogen selectivity (69.6%) at a C/F ratio of 1:15, even with a relatively low Ni loading of 0.67 g per 10 g FOBS. The enhanced performance of 3%Ni/CeO_2 can be attributed to the increased surface area and the synergistic effect of Ni with the CeO_2 support, providing more active sites for hydrogen-producing reactions. Figure 6 depicted that higher C/F ratios consistently enhanced the catalytic performance of 3%Ni/CeO_2, demonstrating the combined importance of Ni modification and appropriate catalyst loading for achieving higher hydrogen yields.

3.2.2. Influence of temperature

The influence of temperature on the pyrolysis process is particularly significant, as thermal energy is essential for breaking the complex molecular structure of the feedstock. In this study, the C/F ratio was fixed at 1:15, as this condition previously showed the best performance in terms of conversion, gas yield, and hydrogen selectivity for the 3%Ni/CeO_2 catalyst. The nitrogen flow rate was maintained at 90 mL/min to ensure a stable reaction environment. The reaction temperature was varied within the range of 400-600 °C, and the resulting conversion, product yields, and hydrogen selectivity are presented in Table 3. Based on Table 3 at 400 °C, a relatively low

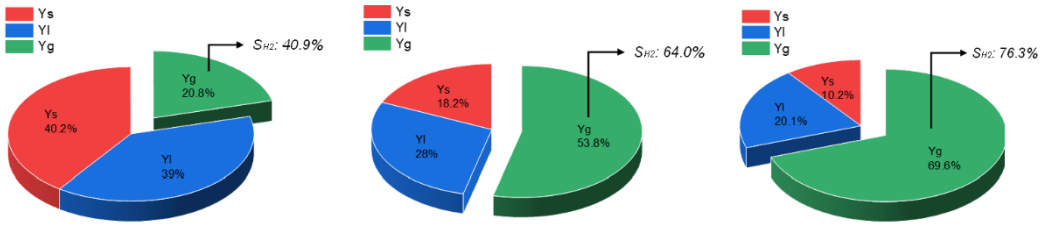

(a) C/F ratio 1:5 (b) C/F ratio 1:10 (c) C/F ratio 1:15

Figure 6. Yields products and selectivity of hydrogen using 3%Ni/CeO_2 at each ratio.

Table 3. Conversion, yield, and selectivity at temperatures 400 °C, 500 °C, and 600 °C.

T (°C)	Catalyst	Conv. (%)	Y_s (%)	Y_l (%)	Y_g (%)	S_{H2} (%)
400	Blank (no catalyst)	48.4	51.6	22.0	26.4	-
	CeO_2	54.7	45.3	34.0	20.7	21.0
	3%Ni/CeO_2	66.8	33.2	24.0	42.8	32.4
500	Blank (no catalyst)	57.7	42.3	20.0	37.7	11.7
	CeO_2	78.9	21.1	30.0	48.9	51.0
	3%Ni/CeO_2	89.8	10.2	20.1	69.6	76.3
600	Blank (no catalyst)	55.6	44.4	36.0	19.6	-
	CeO_2	81.1	18.9	34.0	47.1	60.1
	3%Ni/CeO_2	89.0	11.0	17.0	72.0	78.6

conversion of 48.4% was observed in the blank experiment, accompanied by a gas yield of 26.4% and no hydrogen production. This indicates that the supplied thermal energy was insufficient to effectively decompose the complex molecular structure of FOBS. In conventional pyrolysis within the temperature range of 350 °C-450 °C, the feedstock only begins to break down long and complex hydrocarbon chains, whereas above 450 °C, hydrocarbons undergo more extensive disintegration and molecular rearrangement [5]. Therefore, at 400 °C, the blank experiment lacked adequate energy to fully decompose FOBS and promote complete pyrolytic reactions. According to a previous study, at low temperatures, the energy supplied is often insufficient to break down complex hydrocarbon structures or activate catalytic sites effectively [26].

Then, as the CeO_2 catalyst was introduced to the system, a slight improvement in conversion was observed, increasing to 54.7%. This improvement can be attributed to the oxygen storage capacity and redox properties of ceria, which facilitate cracking reactions. However, the gas yield remained relatively low at 20.7%, with a hydrogen selectivity of 21.0%, indicating limited enhancement in gas-phase reactions at this temperature. In contrast, the 3%Ni/CeO_2 catalyst exhibited a substantial increase in performance, with conversion rising to 66.8%, gas yield increasing to 42.8%, and hydrogen selectivity reaching 32.4%. These results demonstrate a strong synergistic effect between nickel and ceria. This improvement is likely associated with the increased surface area and increased number of active sites provided by the combined Ni-CeO_2 system, which promotes more effective C-C and C-H bond cleavage even at relatively low temperatures. However, according to a previous study, the catalytic activity is still limited, and thermal decomposition alone is insufficient to achieve high hydrogen production. As a result, the cracking of large molecules into smaller hydrogen-rich gases is restricted, and the formation of non-volatile residues or tar-like compounds may dominate [27].

At 500 °C, a significant improvement in conversion, gas yield, and hydrogen selectivity was observed across all systems. For the blank experiment, the conversion increased to 57.7%, accompanied by a gas yield of 37.7% and a hydrogen selectivity of 11.7%. Although hydrogen production remained relatively low, this result represents a clear improvement compared to 400 °C, indicating that increased thermal energy enhances the extent of pyrolytic reactions under non-catalytic conditions. The degradation of complex feedstock structures at elevated temperatures involves simultaneous processes such as dehydration, depolymerization, re-polymerization, fragmentation, rearrangement, and condensation, which collectively promote the formation of smaller molecular compounds [28].

Then, with the presence of catalyst, further improvements were observed. CeO_2 catalyst achieved a high conversion of 78.9% and a gas yield of 48.9%, with hydrogen selectivity reaching 51.0%. Meanwhile, the 3%Ni/CeO_2 catalyst demonstrated the best overall performance, attaining the highest conversion 89.8% and gas yield 69.6%, while minimizing the solid yield to 10.2%. The increase in hydrogen selectivity to 76.3% can be attributed to the combined effects of elevated temperature and the synergistic interaction between nickel and ceria, which enhance catalytic activity and strongly promote secondary reactions such as steam reforming, dry reforming, and the water-gas shift reaction, thereby increasing hydrogen-rich gas production [29].

At 600 °C, the blank experiment showed a slight decrease in conversion compared to 500 °C, with no hydrogen detected. The product distribution shifted toward solids, with solid yield rising to 44.4%, while liquid and gas yields were 36.0% and 19.6%, respectively. For the CeO_2 catalyst, conversion slightly increased to 81.1%, although the gas yield decreased marginally to 47.1%. Interestingly, hydrogen selectivity increased to 60.1%. This apparent contradiction arises because selectivity reflects the proportion of hydrogen in the total gas, not the total gas amount. At higher temperatures, CeO_2 promotes secondary reactions that generate hydrogen, including reforming reactions in Equation (6):

$$C_xH_y + H_2O \rightleftharpoons CO + H_2 \quad (6)$$

and the water gas-shift reactions in Equation (7);

$$CO + H_2O \rightarrow CO_2 + H_2 \quad (7)$$

Meanwhile, the 3%Ni/CeO_2 catalyst maintained a high conversion of 89.0%, with gas yield increasing to 72.0% and hydrogen selectivity reaching 78.6%. The combination of nickel active sites and the oxygen mobility of CeO_2 enhances C-C and C-H bond cleavage and promotes secondary reforming reactions, leading to efficient hydrogen production. Overall, among the temperatures studied, 600 °C provided the highest conversion, gas yield, and hydrogen selectivity, indicating that this temperature is the most favourable for maximizing hydrogen-rich gas production during the catalytic pyrolysis of FOBS. Figure 7 illustrated the overall trends in product yields across the different catalysts and temperatures.

3.2.3. Influence of nitrogen gas flow rate

The nitrogen flow rate is a critical operational parameter in pyrolysis, as it ensures the continuous removal of vaporized products from the reaction zone. An adequate nitrogen flow allows vapors to either condense into liquid products or exit the system as gaseous products. If the nitrogen flow rate is insufficient, the pyrolysis products may remain in the reactor, leading to incomplete separation [30]. Conversely, an excessively high flow rate can destabilize the reaction by sweeping vapors away too quickly, reducing their contact time with the catalyst and limiting reaction efficiency. Figure 8 illustrated the nitrogen gas flow within the pyrolysis system.

The influence of nitrogen flow rate on pyrolysis performance was investigated at a fixed reaction temperature of 600 °C and a catalyst-to-feed (C/F) ratio of 1:15. Nitrogen flow rates of 40, 90, and 140 mL/min were evaluated to elucidate their effects on conversion, product distribution, and hydrogen selectivity under both non-catalytic and catalytic conditions, which are tabulated in Table 4. At the lowest nitrogen flow rate of 40 mL/min, relatively low conversions were observed for the blank experiment (47.9%) and the CeO_2 catalyst (53.4%), indicating insufficient removal of volatile products from the reaction zone. Under these conditions, the prolonged residence time of pyrolysis vapors likely promoted secondary reactions and coke formation, as reflected by the high solid yields of 52.1% and 46.6%, respectively. The introduction of 3% Ni/CeO_2 significantly enhanced conversion to 68.7%, accompanied by a marked reduction in solid yield (31.3%) and an increase in gas yield (58.7%). This improvement highlights the catalyst's role in facilitating C-C and C-H bond cleavage, thereby promoting the further cracking of heavy intermediates into gaseous products. However, hydrogen selectivity (37.9%) remained moderate, suggesting that mass transfer limitations at low nitrogen flow rates still constrained effective hydrogen release.

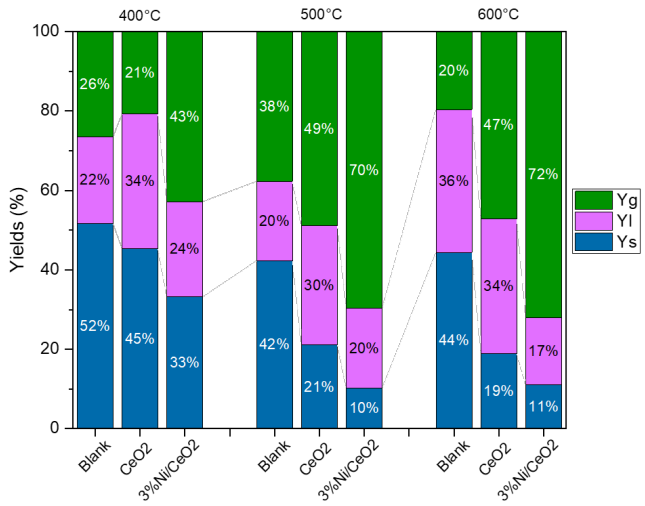

Figure 7. Product trends across catalysts and temperatures.

Increasing the nitrogen flow rate to 90 mL/min resulted in a substantial improvement in overall reaction performance for all systems. The blank experiment showed an increased conversion of 57.7%, while CeO_2 and 3%Ni/CeO_2 achieved significantly higher conversions of 81.1% and 91.2%, respectively. The enhanced nitrogen flow improved the continuous sweeping of volatile products, thereby reducing secondary polymerization reactions and favoring gas-phase product formation. This behavior is evidenced by the sharp decrease in solid yield. Notably, 3%Ni/CeO_2 exhibited the highest hydrogen selectivity (72.2%) at this flow rate, indicating that 90 mL/min represents an optimal balance between vapor residence time and effective product removal.

At the highest nitrogen flow rate of 140 mL/min, the conversion of the blank experiment increased slightly to 60.1%, accompanied by a further reduction in gas yield (28.0%) and a moderate increase in liquid yield (32.1%). This indicates that excessively high nitrogen flow may reduce the residence time of pyrolysis vapors in the reactor, thereby limiting the extent of cracking and gas formation. For the CeO_2 catalyst, conversion remained high at 82.4%, with a significant increase in gas yield (61.4%) compared to the blank, although hydrogen selectivity dropped sharply to 12.0%. This indicates that while CeO_2 continues to promote cracking at high flow rates, the rapid removal of intermediates may limit secondary

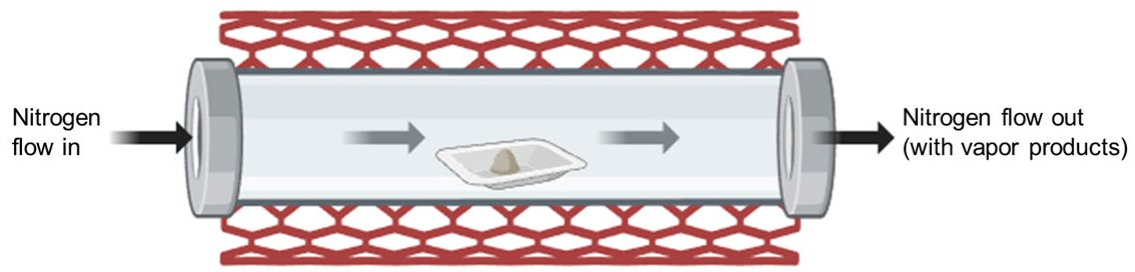

Figure 8. System illustration with nitrogen flow.

dehydrogenation reactions necessary for hydrogen formation. Previous study has reported that as vapors move more quickly through the catalytic bed, the duration available for essential catalytic reactions, particularly cracking, reforming, and dehydrogenation, is significantly shortened, which limits the overall conversion efficiency [31].

For the 3%Ni/CeO_2 catalyst, conversion remained high at 89.0%, with a further increase in gas yield to 72.0% and a corresponding decrease in solid and liquid yields. However, hydrogen selectivity decreased slightly to 48.1% compared to the 90 mL/min condition. This indicates that an excessively high nitrogen flow rate can reduce the contact time between reactive intermediates and active Ni sites, thereby limiting hydrogen production despite efficient overall cracking. Figure 9 further highlighted the effects of nitrogen flow rate on the performance of the 3%Ni/CeO_2 catalyst in terms of conversion, gas yield, and hydrogen selectivity. Increasing the nitrogen flow from 40 to 90 mL/min significantly enhances conversion and hydrogen selectivity, indicating more effective removal of volatile intermediates and improved catalytic cracking. The maximum hydrogen selectivity observed at 90 mL/min suggests an optimal vapor residence time that favors dehydrogenation reactions over Ni active sites. At 140 mL/min, although gas yield continues to increase, hydrogen selectivity declined, implying that excessive carrier gas flow shortened contact time between reactive species and the catalyst surface.

4. Conclusion

This study investigated hydrogen production from fuel oil blended stock (FOBS) via catalytic pyrolysis. The objectives were to synthesize and characterize Ni, CeO_2 and Ni/CeO_2 catalysts and evaluate their performance under different operating conditions. Among the tested catalysts, 3%Ni/CeO_2 exhibited the highest hydrogen yield and gas production. The effects of catalyst-to-feedstock (C/F) ratio, reaction temperature, and nitrogen flow rate were systematically assessed, with the optimal conditions determined as a C/F ratio of 1:15, reaction temperature of 600 °C, and nitrogen flow rate of 90 mL/min. Under these conditions, the 3%Ni/CeO_2 catalyst achieved a conversion of 91.2%, gas yield of 70.2%, and hydrogen selectivity of 72.2%. These results demonstrate that Ni/CeO_2 catalysts effectively enhance hydrogen production from FOBS, thereby fulfilling the objectives of this study.

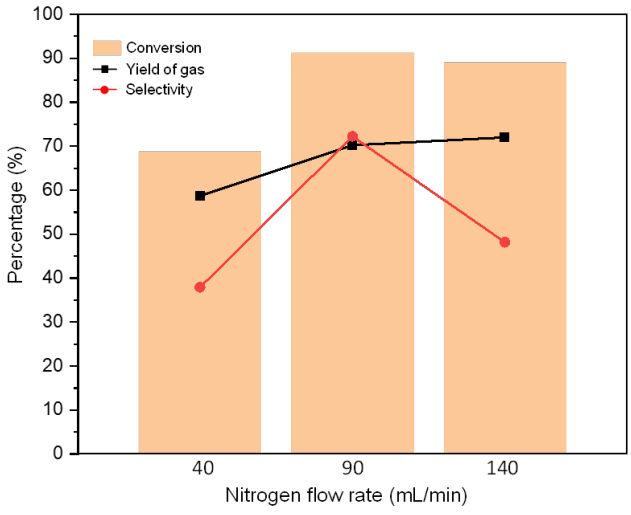

Figure 9. Influence of nitrogen flow rate on hydrogen production performance over 3%Ni/CeO_2 catalyst.

Acknowledgment

The authors would like to extend their most profound appreciation to the Ministry of Higher Education Malaysia (MOHE) for the financial support through the Fundamental Research Grant Scheme (FRGS/1/2020/TK0/UTM/02/97) and Universiti Teknologi Malaysia Fundamental Research (UTMFR) for the financial support under Research University Grant (Vote 23H01).

CRedit Author Statement

Author Contributions: Wan Nur Anis Amira Wan Ranizang: Conceptualization, Methodology, Investigation, Data Curation, Writing, Editing and Revision; Zaki Yamani Zakaria: Project Leader, Supervision, Conceptualization, Methodology, Review and Editing; Mazura Jusoh: Supervision and Review; Mohd Asmadi: Conceptualization, Methodology, Supervision, and Review. All authors have read and agreed to the published version of the manuscript.

References

[1] Sadeq, A.M., Homod, R.Z., Hussein, A.K., Togun, H., Mahmoodi, A., Isleem, H.F., Patil, A.R., Moghaddam, A.H. (2024). Hydrogen energy systems: Technologies, trends, and future prospects. *Science of The Total Environment*, 939, 173622. DOI: 10.1016/J.SCITOTENV.2024.173622.

[2] Ranizang, W.N.A.A.W., Zakaria, Z.Y., Jusoh, M., Mohammed Yussuf, M.A., Sapari, S. (2025). Thermodynamic Analysis of Naphthyl Compounds by Pyrolysis to Hydrogen. *Semarak International Journal of Petroleum and Chemical Engineering*, 3(1), 68-81. DOI: 10.37934/sijpce.3.1.6881.

[3] Teo, M.L., Jusoh, M., Zakaria, Z.Y. (2022). Thermodynamic analysis of fuel oil blended stock (FOBS) model compound, n-eicosane to hydrogen via oxidative cracking. *Chemical Engineering Research and Design*, 178, 340-355. DOI: 10.1016/j.cherd.2021.12.020.

[4] Schüppel, M., Gräbner, M. (2024). Pyrolysis of heavy fuel oil (HFO) - A review on physicochemical properties and pyrolytic decomposition characteristics for application in novel, industrial-scale HFO pyrolysis technology. *Journal of Analytical and Applied Pyrolysis*, 179, 106432. DOI: 10.1016/j.jaap.2024.106432.

[5] Jahirul, M., Rasul, M., Chowdhury, A., Ashwath, N. (2012). Biofuels Production through Biomass Pyrolysis - A Technological Review. *Energies*, 5(12), 4952-5001. DOI: 10.3390/EN5124952.

[6] Jin, H., Hao, J., Yang, J., Guo, J., Zhang, Y., Cao, C., Farooq, A. (2021). Experimental and kinetic modelling study of α-methyl-naphthalene pyrolysis: Part I. Formation of monocyclic aromatics and small species. *Combustion and Flame*, 233, 111587. DOI: 10.1016/j.combustflame.2021.111587.

[7] Lin, B., Wang, J., Huang, Q., Chi, Y. (2017). Effects of potassium hydroxide on the catalytic pyrolysis of oily sludge for high-quality oil product. *Fuel*, 200, 124-133. DOI: 10.1016/j.fuel.2017.03.065.

[8] Demirbas, A., Al-Ghamdi, K., Sen, N., Aslan, A., Alalayah, W.M. (2017). Gasoline- and diesel- like products from heavy oils via catalytic pyrolysis. *Petroleum Science and Technology*, 35(15), 1607-1613. DOI: 10.1080/10916466.2017.1336768

[9] Lv, Q., Wang, L., Jiang, J., Ma, S., Liu, L., Zhou, Z., Liu, L., Wang, X., Bai, J. (2022). Catalytic pyrolysis of oil-based drill cuttings over metal oxides: The product properties and environmental risk assessment of heavy metals in char. *Process Safety and Environmental Protection*, 159, 354-361. DOI: 10.1016/j.psep.2021.12.063

[10] Xiang, L., Li, H., Qu, Q., Lin, F., Yan, B., Chen, G. (2022). In-situ catalytic pyrolysis of heavy oil residue with steel waste to upgrade product quality. *Journal of Analytical and Applied Pyrolysis*, 167, 105676. DOI: 10.1016/j.jaap.2022.105676.

[11] Greluk, M., Gac, W., Rotko, M., Słowik, G., Turczyniak-Surdacka, S. (2021). Co/CeO_2 and Ni/CeO_2 catalysts for ethanol steam reforming: Effect of the cobalt/nickel dispersion on catalysts properties. *Journal of Catalysis*, 393, 159-178. DOI: 10.1016/j.jcat.2020.11.009.

[12] Borges, R.P., Moura, L.G., Kanitkar, S., Spivey, J.J., Noronha, F.B., Hori, C.E. (2021). Hydrogen production by steam reforming of propane using supported nickel over ceria-silica catalysts. *Catalysis Today*, 381, 3-12. DOI: 10.1016/j.cattod.2021.06.024.

[13] Babaei, K., Bozorg, A., Tavasoli, A. (2021). Hydrogen-rich gas production through supercritical water gasification of chicken manure over activated carbon/ceria-based nickel catalysts. *Journal of Analytical and Applied Pyrolysis*, 159, 105318. DOI: 10.1016/j.jaap.2021.105318

[14] Ranizang, W.N.A.A.W., Zakaria, Z.Y., Jusoh, M., Mohammed Yussuf, M.A. (2025). Fuel oil blended stock for carbon product formation via pyrolysis using Ni-Mo/ZSM-5 bimetallic catalyst. *Thermal Science and Engineering Progress*, 64, 103793. DOI: 10.1016/j.tsep.2025.103793

[15] Rui, N., Zhang, X., Zhang, F., Liu, Z., Cao, X., Xie, Z., Zou, R., Senanayake, S.D., Yang, Y., Rodriguez, J.A., Liu, C.-J. (2021). Highly active Ni/CeO_2 catalyst for CO_2 methanation: Preparation and characterization. *Applied Catalysis B: Environmental*, 282, 119581. DOI: 10.1016/j.apcatb.2020.119581.

[16] Nguyen, T., Do, B.L., Nguyen, P.A., Nguyen, T.T.V., Ha, C.A., Hoang, T.C., Luu, C.L. (2024). Nickel/ceria nanorod catalysts for the synthesis of substitute natural gas from CO_2: Effect of active phase loading and synthesis condition. *Journal of Science: Advanced Materials and Devices*, 9(3), 100752. DOI: 10.1016/j.jsamd.2024.100752.

[17] Hargreaves, J.S.J. (2016). Some considerations related to the use of the Scherrer equation in powder X-ray diffraction as applied to heterogeneous catalysts. *Catalysis, Structure & Reactivity*, 2(1-4), 33-37. DOI: 10.1080/2055074X.2016.1252548.

[18] Azam, S., Park, S.-S. (2024). Impact of Biosynthesized CeO_2 Nanoparticle Concentration on the Tribological, Rheological, and Thermal Performance of Lubricating Oil. *Lubricants*, 12(11), 400. DOI: 10.3390/lubricants12110400.

[19] Mohan, V.B., Jayaraman, K., Bhattacharyya, D. (2020). Brunauer-Emmett-Teller (BET) specific surface area analysis of different graphene materials: A comparison to their structural regularity and electrical properties. *Solid State Communications*, 320, 114004. DOI: 10.1016/j.ssc.2020.114004.

[20] Zhang, Q., Liao, X., Liu, S., Wang, H., Zhang, Y., Zhao, Y. (2022). Tuning Particle Sizes and Active Sites of Ni/CeO_2 Catalysts and Their Influence on Maleic Anhydride Hydrogenation. *Nanomaterials*, 12(13), 2156. DOI: 10.3390/nano12132156.

[21] Naderi, M. (2015). Surface Area. In *Progress in Filtration and Separation* (585-608). Elsevier. DOI: 10.1016/B978-0-12-384746-1.00014-8

[22] Nandiyanto, A.B.D., Oktiani, R., Ragadhita, R. (2019). How to Read and Interpret FTIR Spectroscope of Organic Material. *Indonesian Journal of Science and Technology*, 4(1), 97. DOI: 10.17509/ijost.V4I1.15806

[23] Zhang, C., Dabbs, D. M., Liu, L.-M., Aksay, I. A., Car, R., Selloni, A. (2015). Combined Effects of Functional Groups, Lattice Defects, and Edges in the Infrared Spectra of Graphene Oxide. *The Journal of Physical Chemistry C*, 119(32), 18167-18176. DOI: 10.1021/acs.jpcc.5B02727

[24] Arslan, A., Doğu, T. (2016). Effect of calcination/reduction temperature of Ni impregnated CeO_2-ZrO_2 catalysts on hydrogen yield and coke minimization in low temperature reforming of ethanol. *International Journal of Hydrogen Energy*, 41(38), 16752-16761. DOI: 10.1016/j.ijhydene.2016.07.082

[25] Goren, A.Y., Temiz, M., Erdemir, D., Dincer, I. (2025). The role of effective catalysts for hydrogen production: A performance evaluation. *Energy*, 315, 134257. DOI: 10.1016/j.energy.2024.134257

[26] Ranizang, W.N.A.A.W., Yussuf, M.A.M., Mahadhir, M., Jusoh, M., Zakaria, Z.Y. (2022). Catalytic Pyrolysis of Fuel Oil Blended Stock for Bio-Oil Production: A Review. *Chemical Engineering Transactions*, 97, 373-378. DOI: 10.3303/CET2297063.

[27] Rakesh, N., Dasappa, S. (2018). Analysis of tar obtained from hydrogen-rich syngas generated from a fixed bed downdraft biomass gasification system. *Energy Conversion and Management*, 167, 134-146. DOI: 10.1016/j.enconman.2018.04.092.

[28] Dickerson, T., Soria, J. (2013). Catalytic Fast Pyrolysis: A Review. *Energies*, 6(1), 514-538. DOI: 10.3390/EN6010514

[29] Alshareef, R., Nahil, M.A., & Williams, P.T. (2023). Hydrogen Production by Three-Stage (i) Pyrolysis, (ii) Catalytic Steam Reforming, and (iii) Water Gas Shift Processing of Waste Plastic. *Energy & Fuels*, 37(5), 3894-3907. DOI: 10.1021/acs.energyfuels.2C02934

[30] Wulandari, Y.R., Chen, S.S., Hermosa, G.C., Hossain, M.S.A., Yamauchi, Y., Ahamad, T., Alshehri, S.M., Wu, K.C.W., Wu, H.-S. (2020). Effect of N_2 flow rate on kinetic investigation of lignin pyrolysis. *Environmental Research*, 190, 109976. DOI: 10.1016/j.envres.2020.109976

[31] Zaman, C.Z., Pal, K., Yehye, W.A., Sagadevan, S., Shah, S.T., Adebisi, G.A., Marliana, E., Rafique, R.F., Johan, R.B. (2017). Pyrolysis: A Sustainable Way to Generate Energy from Waste. In *Pyrolysis*. InTech. DOI: 10.5772/intechopen.69036.